

Kerr-like effect induced by quantum-metric nematicity

Wenhao Liang,¹ Akito Daido,^{2,1} and K. T. Law^{1,*}

¹*Department of Physics, Hong Kong University of Science and Technology, Clear Water Bay, Hong Kong, China*

²*Department of Physics, Graduate School of Science, Kyoto University, Kyoto 606-8502, Japan*

(Dated: February 24, 2026)

The magneto-optic Kerr effect (MOKE), which describes the rotation and ellipticity of linearly polarized light upon reflection, typically occurs in magnetic materials that break time-reversal (\mathcal{T}) symmetry. Here we theoretically demonstrate that a similar effect can emerge even in two-dimensional nonmagnetic systems with \mathcal{T} symmetry, owing to the nontrivial quantum geometry of electrons. We reveal that the nematicity of the quantum metric, which corresponds to electric quadrupole moment of electron wave packets, gives rise to a Kerr-like effect (KLE) depending on the incident polarization angle. Notably, neither magnetic order nor spin-orbit coupling, which are conventionally considered essential for the MOKE, is required for its emergence. The KLE is demonstrated by using both a minimal tight-binding model and a model for strained MoS₂ with parameters determined by first-principle calculations. This work reveals a quantum-geometric origin for polarization rotation effects beyond the MOKE and offers a distinct approach to probe quantum geometry and multipole moments of electrons.

Introduction.— In 1877, Kerr observed that when linearly polarized light is reflected from a magnet, it transforms into elliptically polarized light with a rotated polarization axis [1]. This MOKE has been studied for over a century in various systems [2–6]. All previously reported systems exhibiting this effect, including ferromagnets [7–20], antiferromagnets [21–27], ferrimagnets [28, 29], and topological materials [30–33], break \mathcal{T} symmetry through spontaneous magnetization or external magnetic fields. The Kerr effect is attributed to this \mathcal{T} symmetry breaking, which generates antisymmetric off-diagonal components in the optical conductivity tensor through the Berry curvature. Additionally, the spin-orbit coupling (SOC) has been considered essential, as it converts the magnetization to the electrons’ orbital motion [21, 22, 34].

In modern studies of optical responses as well as transport and various other phenomena, the concept of quantum geometry has attracted significant attention [35–37]. While the Berry curvature has been extensively studied over the past few decades [38–45], the quantum metric, which measures the distance between neighboring Bloch states in Brillouin zone, has attracted broader attention only recently. The quantum metric has already been shown to play an important role in nonlinear optical responses [46–50], nonlinear transport [51, 52], electrical properties [53, 54], and flat-band superconductivity [55, 56]. However, despite significant interest and research efforts, it still remains challenging to discover novel quantum-geometric effects and to develop methods for its measurement [35, 54, 57].

In this Letter, we challenge the two premises of the Kerr effect, i.e., \mathcal{T} -symmetry breaking and SOC, in light of the quantum geometry of electronic states. We elucidate that the Kerr-like polarization rotation effects can emerge when the system has quantum metric with nematicity, that is, rotational-symmetry breaking [Fig. 1].

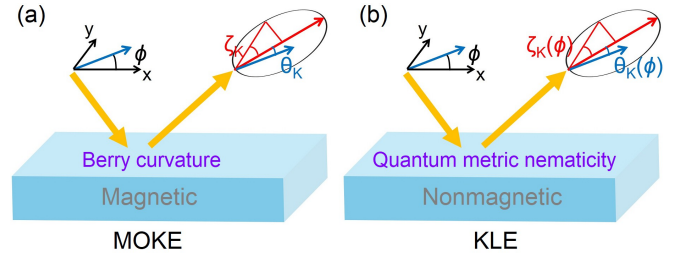


FIG. 1. Schematic figure of the (a) MOKE and (b) KLE. The incident light is affected by (a) the Berry curvature and (b) the quantum-metric nematicity and reflected as an elliptically polarized light, and experiences a polarization rotation θ_K (red arrow) and gains an ellipticity ζ_K , which depends on the incident polarization angle ϕ (blue arrow) only for the KLE.

In contrast to the MOKE, the KLE is dependent on incident polarization. We demonstrate by using a minimal model and a realistic tight-binding model of strained MoS₂ with and without SOC that quantum-metric nematicity is the essential ingredient of the KLE. This makes clear contrast to the MOKE, which has the Berry curvature as its origin. Notably, neither magnetization nor SOC is required for the quantum metric, nor for the resulting polarization rotation and ellipticity.

It should be noted that such polarization rotation effects have been recognized and associated with birefringence and dichroism in the literature of MOKE in anisotropic materials with \mathcal{T} symmetry breaking [19, 20, 27]. However, less attention has been paid to \mathcal{T} -symmetric systems, especially its microscopic origin and its relationship to quantum geometry. Furthermore, our works also answers the question of the methods to observe electric quadrupole moments of electrons. Actually, quantum-metric nematicity corresponds to the electric quadrupole moment of Bloch wave packets, and it has been elusive how to observe it in experiments. Thus,

our work highlights the importance of a previously unexplored effect from the perspective of quantum geometry and multipole moments, establishing it as their useful probe.

Optical conductivity and quantum geometry.—We begin by introducing the optical conductivity with emphasis on the quantum geometric tensor, which incorporates both the Berry curvature and the quantum metric. To illustrate the concept, we focus on two-dimensional insulator at zero temperature in this Letter. Then, the intraband terms can be neglected, and we obtain [58]

$$\sigma_{\alpha\beta}(\omega) = \frac{e^2}{\hbar} \sum_{m \neq n} \int \frac{d\mathbf{k}}{(2\pi)^2} f_m(1-f_n) \frac{\varepsilon_{mn}^2}{\varepsilon_{mn}^2 - (\hbar\omega + i\eta)^2} \times \left(-\frac{\varepsilon_{mn}}{\hbar\omega} \Omega_{\alpha\beta}^{mn} + 2ig_{\alpha\beta}^{mn} \right), \quad (1)$$

where $\Omega_{\alpha\beta}^{mn} = i(A_{\alpha}^{mn}A_{\beta}^{nm} - A_{\beta}^{mn}A_{\alpha}^{nm})$ and $g_{\alpha\beta}^{mn} = \frac{1}{2}(A_{\alpha}^{mn}A_{\beta}^{nm} + A_{\beta}^{mn}A_{\alpha}^{nm})$ denote the band-resolved Berry curvature and quantum metric, respectively. Here, $A_{\alpha}^{mn} = i\langle u_m | \partial_{\alpha} u_n \rangle$ represents the Berry connection, $f_n = 0, 1$ is the Fermi distribution function, $\varepsilon_{mn} = \varepsilon_m - \varepsilon_n$ with ε_n being the energy dispersion for band n , and $\eta \rightarrow 0^+$ is the smearing parameter with units of energy.

From a symmetry perspective, the Berry curvature vanishes on average in \mathcal{T} -symmetric systems. In this case, the optical conductivity is entirely determined by the quantum metric contribution and is a symmetric tensor. The optical conductivity tensor is further constrained by spatial symmetries: For instance, in systems with n -fold rotational symmetry C_{nz} ($n \geq 3$), the relations $\sigma_{xx} = \sigma_{yy}$ and $\sigma_{xy} = -\sigma_{yx}$ are satisfied. This indicates that the rotational symmetry breaking, or nematicity, of the quantum metric plays an important role in nontrivial optical properties.

Rotation angle and ellipticity.—To clarify the quantum-metric effect on reflection, we derive a general formula for the polarization rotation and ellipticity in general two-dimensional materials. Consider normally incident light propagating along the z -direction and linearly polarized in the xy plane at an angle ϕ relative to the x -axis, $\mathbf{E}_i(z, t) = E_i e^{i(qz - \omega t)} \hat{\mathbf{e}}_i$, where $\hat{\mathbf{e}}_i = (\cos \phi, \sin \phi)$. By solving Maxwell's equations and applying boundary conditions at the interface $z = 0$, we obtain the reflection tensor $r_{\alpha\beta}$ by [58]

$$r_{\alpha\beta} = \frac{-Z_0(2\sigma_{\alpha\beta} + Z_0\delta_{\alpha\beta} \det \sigma)}{4 + 2Z_0 \text{tr} \sigma + Z_0^2 \det \sigma}, \quad (2)$$

where $Z_0 = \sqrt{\frac{\mu_0}{\varepsilon_0}}$ is the impedance of the free space, ε_0 is the dielectric constant and μ_0 the permeability in the vacuum. Here, $\sigma_{\alpha\beta} = \sigma_{\alpha\beta}(\omega)$ is the optical conductivity tensor. The reflected electric field can be expressed as $\mathbf{E}_r = rE_i\hat{\mathbf{e}}_i$ with Eq. (2), which generally has components both parallel and perpendicular to the incident

polarization $\hat{\mathbf{e}}_i$ with phase difference (see Supplementary Material [58]). This means that the reflected electric field \mathbf{E}_r becomes elliptically polarized, in contrast to the linearly polarized incident light \mathbf{E}_i .

Having identified the reflected field is elliptically polarized, the complex Kerr angle can be obtained through geometric analysis [58]:

$$\theta_K + i\zeta_K = \frac{-\sigma_H + \bar{\sigma}_{xy} \cos 2\phi - \bar{\sigma}_{x^2-y^2} \sin 2\phi}{\bar{\sigma}_{x^2-y^2} \cos 2\phi + \bar{\sigma}_{xy} \sin 2\phi + \frac{\text{tr} \sigma + Z_0 \det \sigma}{2}}. \quad (3)$$

Here, θ_K represents the rotation angle of the major axis of the reflected light relative to the polarization direction of the incident light, while ζ_K denotes the ratio of the major to minor axis of the polarization ellipse. We can see that the optical conductivity enters through the Hall component $\sigma_H = (\sigma_{xy} - \sigma_{yx})/2$ and longitudinal and transverse anisotropic components $\bar{\sigma}_{x^2-y^2} = (\sigma_{xx} - \sigma_{yy})/2$ and $\bar{\sigma}_{xy} = (\sigma_{xy} + \sigma_{yx})/2$, respectively.

The expression Eq. (3) holds regardless of whether the system has \mathcal{T} symmetry, and shows that the polarization rotation angle generally depends on the incident polarization direction. In systems with C_{nz} ($n \geq 3$) symmetry, the anisotropic components $\bar{\sigma}_{x^2-y^2}$ and $\bar{\sigma}_{xy}$ are prohibited, and θ_K is purely determined by the Hall component and ϕ independent: This corresponds to the conventional MOKE. In turn, even in systems with \mathcal{T} symmetry and $\sigma_H = 0$, we can obtain the Kerr-like rotation as long as $\bar{\sigma}_{x^2-y^2}$ or $\bar{\sigma}_{xy}$ are finite. As can be seen from Eq. (1), these terms can be finite only when the system has the quantum-metric nematicity,

$$\bar{g}_{x^2-y^2}^{mn}(\mathbf{k}) = \frac{g_{xx}^{mn}(\mathbf{k}) - g_{yy}^{mn}(\mathbf{k})}{2}, \quad \bar{g}_{xy}^{mn}(\mathbf{k}) = g_{xy}^{mn}(\mathbf{k}). \quad (4)$$

Thus, observation of the KLE in \mathcal{T} -symmetric systems is the manifestation of the quantum-metric nematicity, in the same way that the MOKE reflects the time-reversal-breaking Berry curvature.

Physically, the quantum-metric nematicity has a direct relationship to the electric quadrupole moments of the Bloch wave packet [59–61] with wave number \mathbf{k} of the band m , which are given by $\sum_{m \neq n} \bar{g}_{x^2-y^2}^{mn}(\mathbf{k})$ and $\sum_{m \neq n} \bar{g}_{xy}^{mn}(\mathbf{k})$, respectively. Since the KLE selectively captures the quantum-metric nematicity contributed by a set of bands satisfying $|\varepsilon_{mn}| \sim \hbar\omega$, it gives a natural probe for the band-wise electric quadrupole moments of Bloch wave packets, whose observation is difficult and hence rarely reported.

KLE in minimal model.—We illustrate the KLE with a minimal tight-binding model on a honeycomb lattice described by the Hamiltonian

$$H = - \sum_{\langle ij \rangle} t_{ij} c_i^\dagger c_j + \sum_i c_i^\dagger \Delta_i c_i, \quad (5)$$

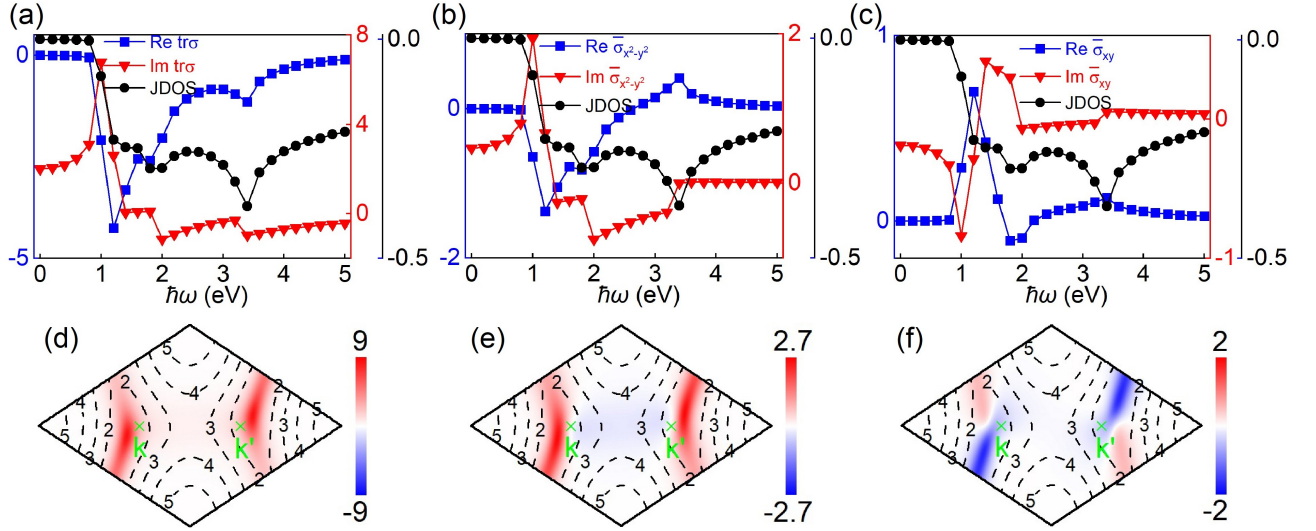


FIG. 2. The optical conductivity (in units of e^2/h) and quantum metric nematicity in the nonmagnetic minimal model. The optical conductivity (a) $\text{tr}\sigma$, (b) $\bar{\sigma}_{x^2-y^2}$, (c) $\bar{\sigma}_{xy}$ and corresponding JDOS with the smearing parameter $\eta = 0.01$. The distribution of quantum metric (d) $\text{tr}g$, (e) $\bar{g}_{x^2-y^2}$, and (f) \bar{g}_{xy} in the first Brillouin zone, with “ \times ” denoting the position of two valleys K and K' . The dashed curve shows the equal energy contour for the optical transition with different photon energy.

with $i, j = A, B$ being the sublattice degrees of freedom. The second term is the sublattice potential $\Delta_A = -\Delta_B = \Delta$, which introduces a mass term to the Dirac points to open the band gap. The first term is the nearest-neighbor hopping with different amplitudes t_1, t_2 , and t_3 for three different directions. This model realizes massive Dirac models with pseudo-gauge fields, and may correspond to graphene coupled to hBN [62] with applied strain [63]. We set $t_1 = 1$ eV as energy unit, $t_2 = 1.2t_1$, $t_3 = 0.6t_1$, and $\Delta = 0.5t_1$.

The model preserves \mathcal{T} symmetry and breaks C_{3z} symmetry. Therefore, the system is allowed to show the KLE, while the MOKE is prohibited. To see this, we first show in Figs. 2(a)–(c) the optical conductivity tensor computed from Eq. (1). Not only the isotropic component $\text{tr}\sigma$ but also the anisotropic components $\bar{\sigma}_{x^2-y^2}$ and $\bar{\sigma}_{xy}$ are finite, reflecting the C_{3z} symmetry breaking. The behavior of the isotropic component $\text{tr}\sigma$ can qualitatively be understood by the joint-density of states (JDOS),

$$\text{JDOS} = \sum_{m \neq n} \int \frac{d\mathbf{k}}{(2\pi)^2} f_{mn} \delta(\varepsilon_{mn} - \hbar\omega). \quad (6)$$

Indeed, the overall spectrum of $\text{tr}\sigma(\omega)$ (blue) is well reproduced by that of JDOS (black) [Fig. 2(a)]. For example, when the photon energy $\hbar\omega$ is smaller than the band gap ≈ 1 eV, JDOS is absent, and therefore $\text{Re}\sigma_{\alpha\beta}(\omega)$ vanishes. We can also see that the peak of $\text{Re}\text{tr}\sigma(\omega)$ at $\hbar\omega = 3.4$ eV follows from that of the JDOS.

On the other hand, the anisotropic components of the optical conductivity $\bar{\sigma}_{x^2-y^2}$ and $\bar{\sigma}_{xy}$ have spectrum much different from JDOS. In contrast to JDOS, which has no sign change, $\text{Re}\bar{\sigma}_{x^2-y^2}$ and $\text{Re}\bar{\sigma}_{xy}$ show sign reversals at $\hbar\omega \approx 2.5$ eV and 1.7 eV in Figs. 2(b) and (c),

respectively. These results clearly illustrate the importance of the quantum metric nematicity in understanding anisotropic components of the optical conductivity.

To clarify the role of quantum metric, we plot its distribution over the Brillouin zone as shown in Fig. 2(d)–(f). In our model, the band gap opens slightly away from the K and K' points due to the strain (the pseudo-gauge field effects), and gives rise to the quantum-metric hot spots nearby. The quantum-metric nematicity $\bar{g}_{x^2-y^2}(\mathbf{k})$ and $\bar{g}_{xy}(\mathbf{k})$ are shown in Figs. 2(e) and (f). They show both positive and negative regions in Brillouin zone, in contrast to the isotropic component $\text{tr}g(\mathbf{k}) \geq 0$ [Fig. 2(d)].

Such a separation of positive and negative quantum-metric nematicity in Brillouin zone accompanies that in energy, and this is essential to understand the behavior of $\bar{\sigma}_{x^2-y^2}$ and $\bar{\sigma}_{xy}$. Indeed, the quantum-metric nematicity averaged over the energy contour $\varepsilon_{mn}(\mathbf{k}) = \hbar\omega$ determines the optical conductivity up to a prefactor and JDOS, as understood from the formula [58]

$$\text{Re}\bar{\sigma}_{x^2-y^2,xy}(\omega) = \pi\omega e^2 [\text{JDOS}] \langle \bar{g}_{x^2-y^2,xy} \rangle_\omega, \quad (7)$$

with the averaged quantum-metric nematicity on the resonant energy contour

$$\langle \bar{g}_{x^2-y^2,xy} \rangle_\omega \equiv \frac{\sum_{m \in \text{occ}, n \notin \text{occ}} \int d\mathbf{k} \delta(\varepsilon_{mn} + \hbar\omega) \bar{g}_{x^2-y^2,xy}^{mn}}{\sum_{m \in \text{occ}, n \notin \text{occ}} \int d\mathbf{k} \delta(\varepsilon_{mn} + \hbar\omega)}. \quad (8)$$

In Fig. 2(e) (Fig. 2(f)), the quantum-metric nematicity changes sign near $\hbar\omega = 2.5$ ($\hbar\omega = 1.7$) eV as can be read out from the energy contours shown by dashed lines. This explains the sign reversals of $\text{Re}\bar{\sigma}_{x^2-y^2}$ and $\text{Re}\bar{\sigma}_{xy}$ in Fig. 2 (b) and (c).

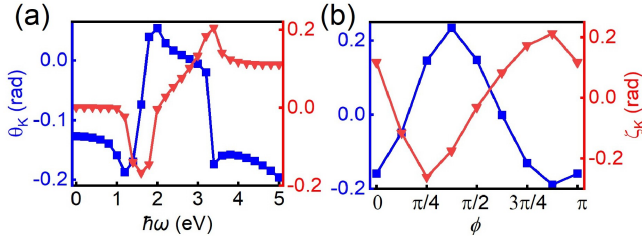


FIG. 3. KLE in nonmagnetic minimal model. The rotation angle θ_K and ellipticity ζ_K (a) versus photon energy $\hbar\omega$ ($\phi = 0$), and (b) versus polarization angle ϕ ($\hbar\omega = 4$ eV).

Next, we discuss the imaginary part of the optical conductivity [red curves in Fig. 2(a)-(c)]. While the imaginary part has a complicated spectrum due to the energy factor in Eq. (1), the quantum-metric nematicity is still required for the anisotropic components $\text{Im}\bar{\sigma}_{x^2-y^2}$ and $\text{Im}\bar{\sigma}_{xy}$ to be finite, as ensured by symmetry. A particularly simple relation between them is obtained when the frequency is much smaller than the band gap, where the optical conductivity is proportional to the quantum-metric nematicity integrated over the Brillouin zone, $\bar{\sigma}_{x^2-y^2,xy}(\omega \rightarrow 0) = (2ie^2/\hbar) \sum_{m \neq n} \int \frac{dk}{(2\pi)^2} \bar{g}_{x^2-y^2,xy}^{mn}$. This corresponds to the quantum weight [64, 65] and provides the finite offset at $\omega = 0$ in Fig. 2(b) and (c). Moreover, it's worth noting that the quantum weight is also related to $\text{Re}\sigma(\omega)$ through the optical sum rule (see Supplementary Material [58]), and thus KLE proves a way to measure the quantum weight.

To quantify the KLE, we discuss the complex Kerr angle $\theta_K + i\zeta_K$. Figure 3(a) shows the ω dependence of θ_K (blue) and ζ_K (red) for a fixed polarization direction $\phi = 0$, where $\bar{\sigma}_{xy}$ is essential according to Eq. (3). When the photon energy is below the band gap, the ellipticity ζ_K vanishes due to the absence of absorption, while the rotation angle θ_K remains finite. As the photon energy increases, the interplay between the quantum metric and the energy factor leads to the evolution of the complex Kerr angle, accompanied by several pronounced peaks. Moreover, increasing the mass term Δ to enlarge the band gap roughly reduces the peak values of Kerr angles [58], as the quantum metric generally decreases with increasing band gap, which also demonstrate the key role of the quantum metric. In Fig. 3(b), we fix the photon energy at $\hbar\omega = 4$ and examine the dependence of the complex Kerr angle on the incident polarization direction $0 \leq \phi \leq \pi$. The KLE is not only obtained at $\phi = 0$ but also at $\phi = \pi/4$, reflecting the fact that both of the quantum-metric nematicity \bar{g}_{xy} and $\bar{g}_{x^2-y^2}$ are finite in our model.

KLE in strained MoS₂.—We established that the KLE emerges owing to the quantum-metric nematicity by using a minimal model, where the system preserves \mathcal{T} symmetry and lacks SOC and thus conventional MOKE is prohibited. To demonstrate its feasibility in a realistic

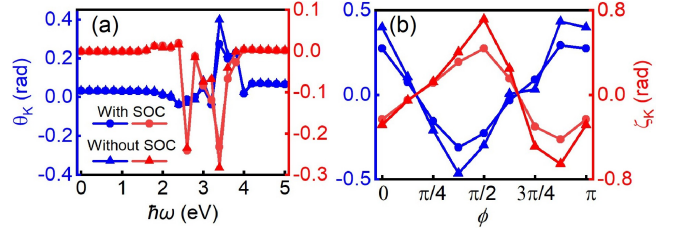


FIG. 4. KLE in strained MoS₂ with and without SOC. The θ_K and ζ_K (a) versus photon energy $\hbar\omega$ ($\phi = 0$), and (b) versus polarization angle ϕ ($\hbar\omega = 3.4$ eV).

material platform, we examine the KLE in monolayer MoS₂ with strain. We adopt a model parametrized from first-principles calculations [58], and the strain effect is taken into account by phenomenologically modifying the hopping parameters as in the previous model, to ensure the presence of the quantum-metric nematicity. The applied strain is estimated to be about 2% [58] and is well achievable in experiments [66].

The results of the KLE are shown in Fig. 4, which are evaluated with and without SOC, respectively. The photon-energy dependence of the complex Kerr angle for the incident polarization angle $\phi = 0$ is shown in Fig. 4(a). Notably, the calculated values of θ_K and ζ_K are nearly identical with and without SOC, demonstrating that SOC plays a negligible role in the obtained Kerr-like response. The sign reversals of θ_K are mainly due to those of the quantum-metric nematicity $\bar{g}_{x^2-y^2}$ and \bar{g}_{xy} , as discussed in details in End Matter. We then fix the photon energy at $\hbar\omega = 3.4$ eV, corresponding to a pronounced peak in both θ_K and ζ_K , and examine the signal as a function of the initial polarization direction ϕ [Fig. 4(b)]. The results remain qualitatively unchanged irrespective of SOC. These findings confirm that a KLE can indeed be realized in realistic transition metal dichalcogenides materials preserving \mathcal{T} symmetry, and that its signature is largely independent of SOC. Furthermore, the magnitude of the obtained KLE lies well within experimentally measurable values by the ellipsometry, an optical technique for characterizing thin-film materials [17, 31, 67, 68]. Thus, the KLE serves as the probe of quantum-metric nematicity in realistic materials.

Discussion—The results obtained in the above demonstrate that the KLE directly occurs as the result of nontrivial quantum geometry, particularly capturing the quantum-metric nematicity of the materials. It has also been demonstrated that the polarization rotation and ellipticity can arise even in nonmagnetic systems with \mathcal{T} symmetry and in the absence of SOC, as the consequence of the quantum-metric nematicity. Besides probing the quantum-metric nematicity, an important application of the KLE is to detect the nematic transition of the system and visualization of nematic domains [19]. When the system is in a rotational-symmetric phase at high tem-

perature but transitions to an anisotropic phase at low temperature, $\bar{\sigma}_{xy}$ and $\bar{\sigma}_{x^2-y^2}$ serve as an order parameter to quantify the nematic phase [58]. They describe different symmetries, corresponding to different types of electric quadrupole moments, and can be selectively probed by the KLE for $\phi = 0$ and $\phi = \pi/4$, respectively. Thus, the KLE offers a contact-free probe of the nematic order and the quantum-metric nematicity brought with it.

We thank Wenyu He, Yingming Xie, Xunjiang Luo and Xilin Feng for valuable discussions. A.D. thanks Cheng-Cheng Liu and Shingo Yonezawa for helpful email correspondence. AD is supported by JSPS KAKENHI (Grant No. JP21K13880, JP23K17353, JP24H01662, JP23KK0248). K.T.L acknowledges the support from the Ministry of Science and Technology, China, and Hong Kong Research Grant Council through Grants No. 2020YFA0309600, No. RFS2021-6S03, No. C6025-19G, No. AoE/P-701/20, No. 16310520, No. 16307622, and No. 16309223.

* Contact author: phlaw@ust.hk

- [1] J. Kerr, On rotation of the plane of polarization by reflection from the pole of a magnet, *Lond. Edinb. Dubl. Phil. Mag. J. Sci.* **3**, 321 (1877).
- [2] P. Weinberger, John kerr and his effects found in 1877 and 1878, *Phil. Mag. Lett.* **88**, 897 (2008).
- [3] H. Feil and C. Haas, Magneto-optical kerr effect, enhanced by the plasma resonance of charge carriers, *Phys. Rev. Lett.* **58**, 65 (1987).
- [4] P. S. Pershan, Magneto-optical effects, *J. Appl. Phys.* **38**, 1482 (1967).
- [5] Z. Q. Qiu and S. D. Bader, Surface magneto-optic kerr effect, *Rev. Sci. Instrum.* **71**, 1243 (2000).
- [6] D. Budker, W. Gawlik, D. F. Kimball, S. M. Rochester, V. V. Yashchuk, and A. Weis, Resonant nonlinear magneto-optical effects in atoms, *Rev. Mod. Phys.* **74**, 1153 (2002).
- [7] P. N. Argyres, Theory of the faraday and kerr effects in ferromagnetics, *Phys. Rev.* **97**, 334 (1955).
- [8] J. L. Erskine and E. A. Stern, Magneto-optic kerr effect in ni, co, and fe, *Phys. Rev. Lett.* **30**, 1329 (1973).
- [9] W. Hübner and K.-H. Bennemann, Nonlinear magneto-optical kerr effect on a nickel surface, *Phys. Rev. B* **40**, 5973 (1989).
- [10] J. Hamrle, J. Ferré, M. Nývlt, and Š. Višňovský, In-depth resolution of the magneto-optical kerr effect in ferromagnetic multilayers, *Phys. Rev. B* **66**, 224423 (2002).
- [11] D. Kim, Y.-W. Oh, J. U. Kim, S. Lee, A. Baucour, J. Shin, K.-J. Kim, B.-G. Park, and M.-K. Seo, Extreme anti-reflection enhanced magneto-optic kerr effect microscopy, *Nat. Commun.* **11**, 5937 (2020).
- [12] G. Y. Guo and H. Ebert, Band-theoretical investigation of the magneto-optical kerr effect in fe and co multilayers, *Phys. Rev. B* **51**, 12633 (1995).
- [13] G. Y. Guo and H. Ebert, Theoretical investigation of the orientation dependence of the magneto-optical kerr effect in co, *Phys. Rev. B* **50**, 10377 (1994).
- [14] M. Kim, A. J. Freeman, and R. Wu, Surface effects and structural dependence of magneto-optical spectra: Ultrathin Co films and CoPt_n alloys and multilayers, *Phys. Rev. B* **59**, 9432 (1999).
- [15] A. Stroppa, S. Picozzi, A. Continenza, M. Kim, and A. J. Freeman, Magneto-optical properties of (ga,mn)as: Anab initiodetermination, *Phys. Rev. B* **77**, 035208 (2008).
- [16] P. Ravindran, A. Delin, P. James, B. Johansson, J. M. Wills, R. Ahuja, and O. Eriksson, Magnetic, optical, and magneto-optical properties of MnX (X=As, Sb, or Bi) from full-potential calculations, *Phys. Rev. B* **59**, 15680 (1999).
- [17] B. Huang, G. Clark, E. Navarro-Moratalla, D. R. Klein, R. Cheng, K. L. Seyler, D. Zhong, E. Schmidgall, M. A. McGuire, D. H. Cobden, W. Yao, D. Xiao, P. Jarillo-Herrero, and X. Xu, Layer-dependent ferromagnetism in a van der waals crystal down to the monolayer limit, *Nature* **546**, 270 (2017).
- [18] I. Lyalin, S. Alikhah, M. Berritta, P. M. Oppeneer, and R. K. Kawakami, Magneto-optical detection of the orbital hall effect in chromium, *Phys. Rev. Lett.* **131**, 156702 (2023).
- [19] Y. Xu, Z. Ni, Y. Liu, B. R. Ortiz, Q. Deng, S. D. Wilson, B. Yan, L. Balents, and L. Wu, Three-state nematicity and magneto-optical kerr effect in the charge density waves in kagome superconductors, *Nat. Phys.* **18**, 1470 (2022).
- [20] H. Rathgen, M. I. Katsnelson, O. Eriksson, and G. Zwicknagl, Polar magneto-optical kerr effect for low-symmetric ferromagnets, *Phys. Rev. B* **72**, 014451 (2005).
- [21] N. Sivadas, S. Okamoto, and D. Xiao, Gate-controllable magneto-optic kerr effect in layered collinear antiferromagnets, *Phys. Rev. Lett.* **117**, 267203 (2016).
- [22] W. Feng, G.-Y. Guo, J. Zhou, Y. Yao, and Q. Niu, Large magneto-optical kerr effect in non-collinear antiferromagnets Mn₃X (X=Rh, Ir, Pt), *Phys. Rev. B* **92**, 144426 (2015).
- [23] Y. Li, Y. Liu, and C.-C. Liu, Quantum metric induced magneto-optical effects in \mathcal{PT} -symmetric antiferromagnets, [arXiv:2503.04312](https://arxiv.org/abs/2503.04312).
- [24] J. Ahn, S.-Y. Xu, and A. Vishwanath, Theory of optical axion electrodynamics and application to the kerr effect in topological antiferromagnets, *Nat. Commun.* **13**, 7615 (2022).
- [25] T. Higo, H. Man, D. B. Gopman, L. Wu, T. Koretsune, O. M. J. van 't Erve, Y. P. Kabanov, D. Rees, Y. Li, M.-T. Suzuki, S. Patankar, M. Ikhlas, C. L. Chien, R. Arita, R. D. Shull, J. Orenstein, and S. Nakatsuji, Large magneto-optical kerr effect and imaging of magnetic octupole domains in an antiferromagnetic metal, *Nat. Photonics* **12**, 73 (2018).
- [26] W. Feng, J.-P. Hanke, X. Zhou, G.-Y. Guo, S. Blügel, Y. Mokrousov, and Y. Yao, Topological magneto-optical effects and their quantization in noncoplanar antiferromagnets, *Nat. Commun.* **11**, 118 (2020).
- [27] S. Iguchi, Y. Ikemoto, H. Kobayashi, H. Kitazawa, H. Itoh, S. Iwai, T. Moriwaki, and T. Sasaki, Infrared magneto-optical kerr effect measurements by polarization modulation method in anisotropic magnets, *Proceedings of the 29th International Conference on Low Temperature* [10.7566/jpscp.38.011148](https://doi.org/10.7566/jpscp.38.011148) (2023).
- [28] K. Fleischer, N. Thiagarajah, Y.-C. Lau, D. Betto, K. Borisov, C. C. Smith, I. V. Shvets, J. M. D. Coey, and K. Rode, Magneto-optic kerr effect in a spin-polarized zero-moment ferrimagnet,

- Phys. Rev. B* **98**, 134445 (2018).
- [29] F. Johnson, J. Zázvorka, L. Beran, D. Boldrin, L. F. Cohen, J. Zemen, and M. Veis, Room-temperature weak collinear ferrimagnet with symmetry-driven large intrinsic magneto-optic signatures, *Phys. Rev. B* **107**, 014404 (2023).
- [30] W.-K. Tse and A. H. MacDonald, Magneto-optical faraday and kerr effects in topological insulator films and in other layered quantized hall systems, *Phys. Rev. B* **84**, 205327 (2011).
- [31] X. Li, C. Liu, Y. Zhang, S. Zhang, H. Zhang, Y. Zhang, W. Meng, D. Hou, T. Li, C. Kang, F. Huang, R. Cao, D. Hou, P. Cui, W. Zhang, T. Min, Q. Lu, X. Xu, Z. Sheng, B. Xiang, and Z. Zhang, Topological kerr effects in two-dimensional magnets with broken inversion symmetry, *Nat. Phys.* **20**, 1145 (2024).
- [32] Y. D. Kato, Y. Okamura, M. Hirschberger, Y. Tokura, and Y. Takahashi, Topological magneto-optical effect from skyrmion lattice, *Nat. Commun.* **14**, 5416 (2023).
- [33] A. Habibi, A. Z. Musthofa, E. Adibi, J. Ekström, T. L. Schmidt, and E. H. Hasdeo, Kerr and faraday rotations in topological flat and dispersive band structures, *New J. Phys.* **24**, 063003 (2022).
- [34] H. Ebert, Magneto-optical effects in transition metal systems, *Rep. Prog. Phys.* **59**, 1665 (1996).
- [35] P. Törmä, Essay: Where can quantum geometry lead us?, *Phys. Rev. Lett.* **131**, 240001 (2023).
- [36] W. Chen and G. von Gersdorff, Measurement of interaction-dressed berry curvature and quantum metric in solids by optical absorption, *SciPost Phys. Core* **5**, 040 (2022).
- [37] R. Resta, The insulating state of matter: a geometrical theory, *Eur. Phys. J. B* **79**, 121 (2011).
- [38] C.-Z. Chang, C.-X. Liu, and A. H. MacDonald, Colloquium : Quantum anomalous hall effect, *Rev. Mod. Phys.* **95**, 011002 (2023).
- [39] W. Liang, Z. Li, J. An, Y. Ren, Z. Qiao, and Q. Niu, Chern number tunable quantum anomalous hall effect in compensated antiferromagnets, *Phys. Rev. Lett.* **134**, 116603 (2025).
- [40] M. Z. Hasan and C. L. Kane, Colloquium: Topological insulators, *Rev. Mod. Phys.* **82**, 3045 (2010).
- [41] I. Sodemann and L. Fu, Quantum nonlinear hall effect induced by berry curvature dipole in time-reversal invariant materials, *Phys. Rev. Lett.* **115**, 216806 (2015).
- [42] W. Liang, T. Hou, J. Zeng, Z. Liu, Y. Han, and Z. Qiao, Layer-dependent zero-line modes in antiferromagnetic topological insulators, *Phys. Rev. B* **107**, 075303 (2023).
- [43] D. Xiao, M.-C. Chang, and Q. Niu, Berry phase effects on electronic properties, *Rev. Mod. Phys.* **82**, 1959 (2010).
- [44] S.-K. Bac, F. Le Mardelé, J. Wang, M. Ozerov, K. Yoshimura, I. Mohelský, X. Sun, B. A. Piot, S. Wimmer, A. Ney, T. Orlova, M. Zhukovskiy, G. Bauer, G. Springholz, X. Liu, M. Orlita, K. Park, Y.-T. Hsu, and B. A. Assaf, Probing berry curvature in magnetic topological insulators through resonant infrared magnetic circular dichroism, *Phys. Rev. Lett.* **134**, 016601 (2025).
- [45] W. Liang, J. Zeng, Z. Qiao, Y. Gao, and Q. Niu, Berry-curvature engineering for nonreciprocal directional dichroism in two-dimensional antiferromagnets, *Phys. Rev. Lett.* **131**, 256901 (2023).
- [46] J. Ahn, G.-Y. Guo, N. Nagaosa, and A. Vishwanath, Riemannian geometry of resonant optical responses, *Nat. Phys.* **18**, 290 (2021).
- [47] H.-C. Hsu, J.-S. You, J. Ahn, and G.-Y. Guo, Nonlinear photoconductivities and quantum geometry of chiral multifold fermions, *Phys. Rev. B* **107**, 155434 (2023).
- [48] T. Holder, D. Kaplan, and B. Yan, Consequences of time-reversal-symmetry breaking in the light-matter interaction: Berry curvature, quantum metric, and diabatic motion, *Phys. Rev. Research* **2**, 033100 (2020).
- [49] J. Ahn, G.-Y. Guo, and N. Nagaosa, Low-frequency divergence and quantum geometry of the bulk photovoltaic effect in topological semimetals, *Phys. Rev. X* **10**, 041041 (2020).
- [50] B. Ghosh, Y. Onishi, S.-Y. Xu, H. Lin, L. Fu, and A. Bansil, Probing quantum geometry through optical conductivity and magnetic circular dichroism, *Sci. Adv.* **10**, eado1761 (2024).
- [51] A. Gao, Y.-F. Liu, J.-X. Qiu, B. Ghosh, T. V. Trevisan, Y. Onishi, C. Hu, T. Qian, H.-J. Tien, S.-W. Chen, M. Huang, D. Bérubé, H. Li, C. Tzschaschel, T. Dinh, Z. Sun, S.-C. Ho, S.-W. Lien, B. Singh, K. Watanabe, T. Taniguchi, D. C. Bell, H. Lin, T.-R. Chang, C. R. Du, A. Bansil, L. Fu, N. Ni, P. P. Orth, Q. Ma, and S.-Y. Xu, Quantum metric nonlinear hall effect in a topological antiferromagnetic heterostructure, *Science* **381**, 181 (2023).
- [52] N. Wang, D. Kaplan, Z. Zhang, T. Holder, N. Cao, A. Wang, X. Zhou, F. Zhou, Z. Jiang, C. Zhang, S. Ru, H. Cai, K. Watanabe, T. Taniguchi, B. Yan, and W. Gao, Quantum-metric-induced nonlinear transport in a topological antiferromagnet, *Nature* **621**, 487 (2023).
- [53] I. Komissarov, T. Holder, and R. Queiroz, The quantum geometric origin of capacitance in insulators, *Nat. Commun.* **15**, 4621 (2024).
- [54] N. Verma and R. Queiroz, Framework to measure quantum metric from step response, *Phys. Rev. Lett.* **134**, 106403 (2025).
- [55] S. A. Chen and K. Law, Ginzburg-landau theory of flat-band superconductors with quantum metric, *Phys. Rev. Lett.* **132**, 026002 (2024).
- [56] X. Guo, X. Ma, X. Ying, and K. Law, Majorana zero modes in the lieb-kitaev model with tunable quantum metric, *Phys. Rev. Lett.* **135**, 076601 (2025).
- [57] D. Bałut, B. Bradlyn, and P. Abbamonte, Quantum entanglement and quantum geometry measured with inelastic x-ray scattering, *Phys. Rev. B* **111**, 125161 (2025).
- [58] See *Supplementary Material*, which includes Ref.[64–66, 68–73].
- [59] Y. Gao and D. Xiao, Nonreciprocal directional dichroism induced by the quantum metric dipole, *Phys. Rev. Lett.* **122**, 227402 (2019).
- [60] Y. Gao, S. A. Yang, and Q. Niu, Geometrical effects in orbital magnetic susceptibility, *Phys. Rev. B* **91**, 214405 (2015).
- [61] M. F. Lapa and T. L. Hughes, Semiclassical wave packet dynamics in nonuniform electric fields, *Phys. Rev. B* **99**, 121111 (2019).
- [62] G. Giovannetti, P. A. Khomyakov, G. Brocks, P. J. Kelly, and J. van den Brink, Substrate-induced band gap in graphene on hexagonal boron nitride:ab initiodensity functional calculations, *Phys. Rev. B* **76**, 073103 (2007).
- [63] S.-M. Choi, S.-H. Jhi, and Y.-W. Son, Effects of strain on electronic properties of graphene, *Phys. Rev. B* **81**, 081407 (2010).
- [64] Y. Onishi and L. Fu, Fundamental bound on topological gap, *Phys. Rev. X* **14**, 011052 (2024).

- [65] Y. Onishi and L. Fu, Quantum weight: A fundamental property of quantum many-body systems, *Phys. Rev. Research* **7**, 023158 (2025).
- [66] S. Manzeli, D. Ovchinnikov, D. Pasquier, O. V. Yazyev, and A. Kis, 2D transition metal dichalcogenides, *Nat. Rev. Mater.* **2**, 17033 (2017).
- [67] V. Choudhury, C. Khandekar, A. K. Boddeti, A. Jishi, M. Erkovan, T. Sentz, F. Kalhor, S. Cardoso, V. R. Supradeepa, and Z. Jacob, Computational kerr ellipsometry: Quantifying broadband optical nonreciprocity of magneto-optic materials, *Phys. Rev. B* **109**, 054433 (2024).
- [68] R. M. Azzam, R. M. A.-G. Azzam, and N. M. Bashara, *Ellipsometry and polarized light*, repr. 1989 ed., edited by N. M. Bashara, North-Holland personal library (North-Holland, Amsterdam [u.a.], 1989).
- [69] M. P. Marder, *Condensed matter physics*, second edition ed. (Wiley, Hoboken, New Jersey, 2010).
- [70] M. Born, *Principles of optics*, seventh (expanded) edition, 13th printing ed., edited by E. Wolf and A. B. Bhatia (Cambridge University Press, Cambridge [u.a.], 2017).
- [71] G.-B. Liu, W.-Y. Shan, Y. Yao, W. Yao, and D. Xiao, Three-band tight-binding model for monolayers of group-vib transition metal dichalcogenides, *Phys. Rev. B* **88**, 085433 (2013).
- [72] C. Li and J. J. He, Microscopic study of supercurrent diode effect in chiral nanotubes, *Phys. Rev. B* **111**, 224504 (2025).
- [73] H. Rostami, R. Roldán, E. Cappelluti, R. Asgari, and F. Guinea, Theory of strain in single-layer transition metal dichalcogenides, *Phys. Rev. B* **92**, 195402 (2015).

End Matter

Results of the optical conductivity and quantum metric nematicity in strained MoS₂

We use the model for monolayer MoS₂ from previous study with parameters determined by first-principle calculations[58]. The band structure has a gap at K point with spin splitting due to the SOC as shown in Fig. 5(a). Due to the highly localized distribution of the quantum metric across the Brillouin zone, we plot the logarithm of the quantum metric to resolve its spatial variation more clearly. The anisotropy of the system manifests in finite $\bar{g}_{x^2-y^2}$ and \bar{g}_{xy} displayed in Fig. 5(c) and (d), respectively. Correspondingly, the optical conductivity $\text{tr}\sigma$, $\bar{\sigma}_{x^2-y^2}$, and $\bar{\sigma}_{xy}$ are shown in Fig. 5(e)-(g). Together with the energy weight factor and the JDOS, quantum metric nematicity gives both the peaks and the sign change of the optical conductivity. In addition, consistent with the results from the minimal model discussed earlier, the optical conductivity is negligibly small for photon energies smaller than the band gap.

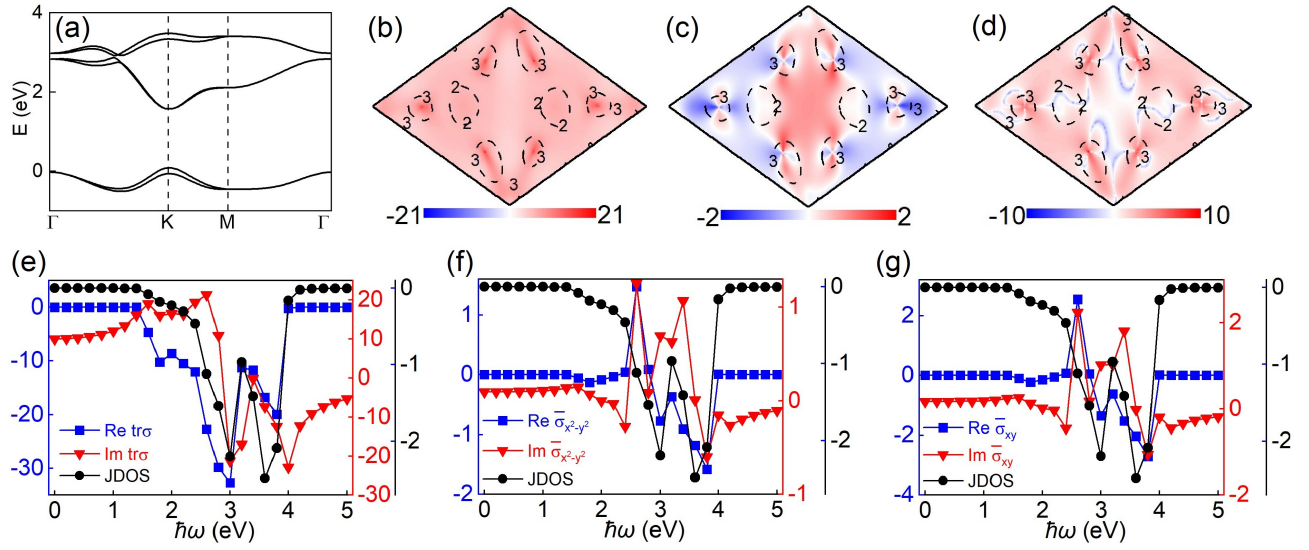


FIG. 5. The quantum metric nematicity and optical conductivity (in units of e^2/h) in strained MoS₂. (a) The band structure along the high symmetry lines. The distribution of the logarithm of the quantum metric (b) $\text{tr}g$, (c) $\bar{g}_{x^2-y^2}$, and (d) \bar{g}_{xy} in the first Brillouin zone. The optical conductivity (e) $\text{tr}\sigma$, (f) $\bar{\sigma}_{x^2-y^2}$, (g) $\bar{\sigma}_{xy}$ and corresponding JDOS.